Journal of Seismology **8:** 247–257, 2004.

Modeling the M_L4.7 mainshock of the February-July 2001 earthquake sequence in Aegion, Greece

J. Zahradník[1], J. Janský[1], E. Sokos[2], A. Serpetsidaki[2], H. Lyon-Caen[3] & P. Papadimitriou[4]
[1]*Faculty of Mathematics & Physics, Charles University in Prague, Czech Republic (e-mail: jz@karel.troja.mff.cuni.cz);* [2]*Seismological Laboratory, University of Patras, Greece;* [3]*Laboratoire de Géologie, Ecole Normale Supérieure, Paris, France;* [4]*Seismological Laboratory, National & Kapodistrian University of Athens, Greece*

Received 13 January 2003; accepted in revised form 17 October 2003

Key words: ASPO method, Corinth Rift, focal mechanism, polarities, waveforms

Abstract

An earthquake sequence comprising almost 2000 events occurred in February-July 2001 on the southern coast of the Corinth Gulf. Several location methods were applied to 171 events recorded by the regional network PATNET. The unavailability of S-wave readings precluded from reliable depth determination. For the mainshock of April 8, M_L = 4.7, the depth varied from 0 to 20 km. The amplitude spectra of complete waveforms at three local stations (KER, SER, DES; epicentral distances 17, 26 and 56 km) were inverted between 0.1 and 0.2 Hz for double-couple focal mechanism and also for the depth. The optimum solution (strike 220°, dip 40°, rake –160°, and depth of 8 km) was validated by forward waveform modeling. Additionally, the mainshock depth was further supported by the P- and S-wave arrival times from the local short-period network CRLNET (Corinth Rift Laboratory). The scalar seismic moment was 2.5e15 Nm, and the moment rate function was successfully simulated by a triangle of the 0.5 second duration. This is equivalent to a 1–1.5 km fault length, and a static stress drop 2–6 MPa. This value is important for future strong ground motion simulation of damaging earthquakes in Aegion region, whose subevents may be modeled according to the studied event. The T axis of the mainshock (azimuth 176° and plunge 67°), is consistent with the regional direction of extension ∼N10°. However, none of the nodal planes can be associated to an active structure seen at the surface. The relationship of this earthquake sequence with deeper faults (e.g. possible detachment at about 10 km) is also unclear.

Introduction

The Corinth Gulf, Greece, is a well known active rift (e.g. Armijo et al., 1996), presently opening at a rate of 1 to 1.5 cm/yr (e.g. Clarke et al., 1997; Briole et al., 2000). Major surface tectonic elements are the ESE-WNW oriented normal faults, steeply dipping to the NNE. The recent seismicity in the western part of the Gulf is very high. On June 15, 1995 a damaging M_L 6.2 earthquake struck the city of Aegion (Tselentis et al., 1996). Modeling the seismic and GPS observations (Bernard et al., 1997) has lead to the conclusion that the 1995 event ruptured a low-angle dipping fault below the Corinth Gulf. The co-existence of high- and low-angle dipping faults in the region is still subject of diverse interpretations (e.g., Rigo et al., 1996; Hatzfeld et al., 2000). It has been suggested that the low-angle dipping faults may correspond to a detachment zone on which the major high-angle dipping faults are rooting and weak events cluster at the crossing between this zone and the major high-angle faults (Rietbrock et al., 1996; Rigo et al., 1996; Lyon-Caen and Rigo, 1997). Alternatively, Hatzfeld et al. (2000) consider that the low-angle dipping faults represent the natural evolution of active normal faults. Complex investigation of the region in the framework of the so-called Corinth Rift Laboratory (CRLNET) EC project cluster is in progress (http://www.corinth-rift-lab.org/). The present paper devoted to the earthquake sequence of February–July

2001, which occurred about 10 km south of the city of Aegion, may also contribute to the understanding of the complex tectonics of the region. As a byproduct, any information about active faults in the inhabited area of the western Corinth Gulf is of importance for building realistic seismic scenarios of future damaging earthquakes there.

In this paper we concentrate on the mainshock of the February-July 2001 sequence (April 8, M_L = 4.7 at 06:12:24 GMT). A detailed study of the entire sequence will be presented elsewhere (Pacchiani et al., in preparation). We focus on some methodological aspects, in particular on the problematic depth determination when using a regional network with enough good P-wave readings, but absent S-wave readings. The first-motion focal mechanism may be also problematic when using stations at larger distances, in the studied magnitude range (M<5). We show how the depth and focal mechanism can be well constrained by analyzing a few waveforms of three-component local stations. To that goal, data of two seismic networks are combined in this paper (PATNET, CRLNET), supplemented by one station of the CORNET network, and two temporary strong-motion stations.

Location by a regional network

The Aegion sequence comprised of about 2000 events. Studied here are 171 events with magnitudes M_L from 1.8 to 4.7, recorded and located by the short-period permanent network PATNET operated in western Greece by the University of Patras (Tselentis et al., 1996; http://seismology.upatras.gr). Those data included 1159 P- and 208 S-wave first arrival readings at 16 vertical-component (Teledyne) stations and one (UNI) 3-component station (Figure 1). The sequence was located by HYPO71PC code of Lee and Valdes (1989), with several starting depths, and by the grid search code of Janský (2000). Several crustal models were used. Besides attempting to employ all stations and events, several subsets of stations and events were also tested. Basically, all these approaches provided very similar distribution of epicenters, but the depth determination was unstable, ranging from 0 to 20 km, most likely due to the unavailability of S-wave readings. Figure 1 shows the epicenters for the simplest case of the HYPO location of the whole studied set of 171 events, using all available stations, starting depth of 7 km, and the crustal model MF (described below). The MF model has also been used in this paper to model spectra and waveforms. The mainshock epicenter of the PATNET location is listed in the first row of Table 1. More details will be published by Janský et al. (submitted).

Table 1. Location of the April 8, 2001 mainshock by two nearest networks, PATNET and CRLNET, discussed in this paper. For comparison, location by the all-Greece network of the National Observatory of Athens (NOA) and by the USGS-NEIC agency are also shown. The Swiss SED center gives the same epicenter as USGS, and reports moment tensor solution from 33 regional stations, whose 90% double-couple part has strike 247°, dip 43° and rake –104°, depth of 18 km, and scalar moment of 9.96e15 Nm

Network	Latitude (°)	Longitude (°)	Depth (km)
PATNET	38.17	22.05	–
CRLNET	38.19	22.03	5.7
NOA	38.16	22.02	5. (fixed)
USGS	38.23	22.06	10. (fixed)

Source parameters from waveforms at local stations

The focal mechanism of the mainshock was calculated by a recently developed method based on *a*mplitude *s*pectra of complete 3-component waveforms, and first-motion *po*larities, hence the ASPO acronym (Zahradník et al., 2001; Zahradník, 2002). The waveforms of three local stations (Figure 2) were employed. The two nearest stations were KER (Kernitsa) and SER (Sergoula), jointly operated in the Corinth Gulf by the University of Patras and the Charles University in Prague. They are equipped, in addition to broad-band seismometers, with digital accelerometers CMG5-T (Guralp). For details, see http://seis30.karlov.mff.cuni.cz. The third station providing waveforms was DES (Desfina), belonging to the CORNET network operated by the University of Athens, equipped with the 3D-Le/5sec (Lennartz); http://www.geophysics.geol.uoa.gr.

All records were instrumentally corrected, resampled into common time increment of 0.01 sec, and high-passed for frequencies $f > 0.1$ Hz. Good signal-to-noise ratio was found up to frequencies as low as 0.1–0.2 Hz. This is important for the success of the focal mechanism inversion since at the lowest frequen-

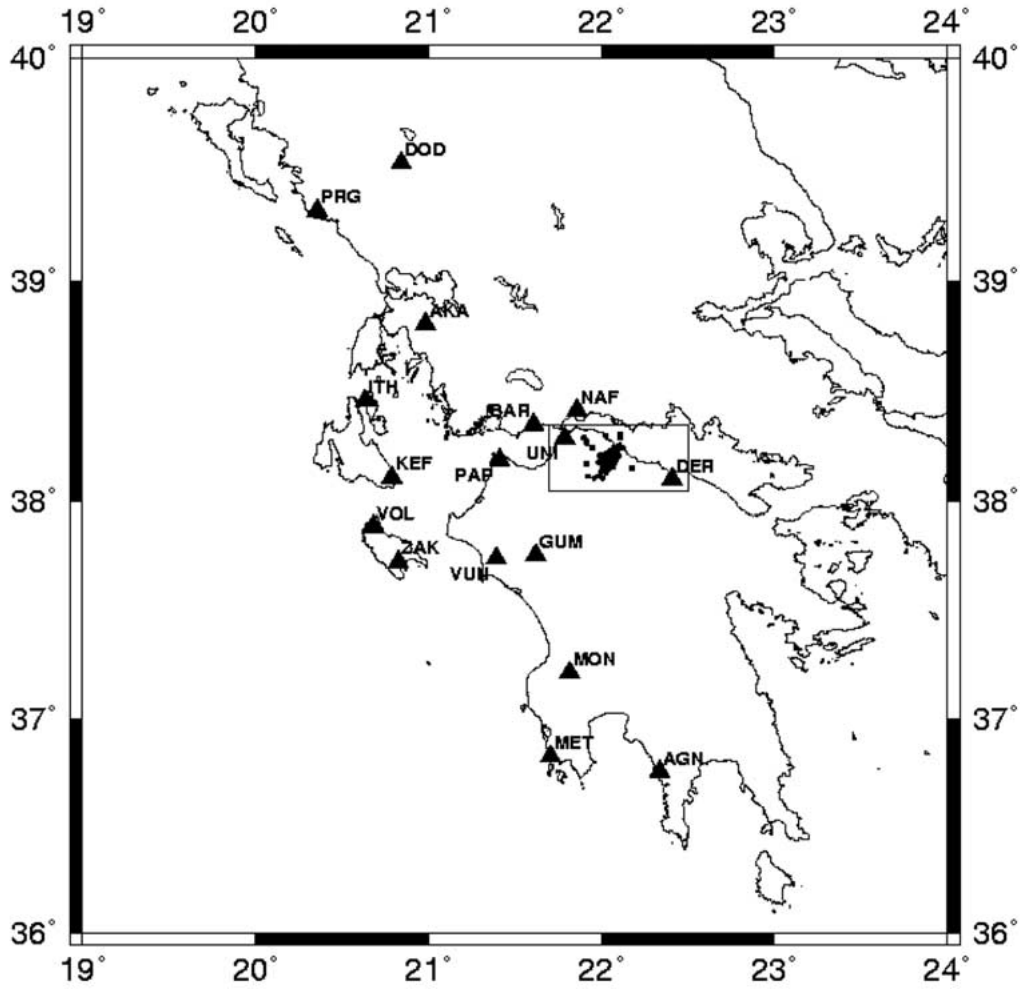

Figure 1. a. Western Greece with 17 PATNET stations (triangles) and the epicenters of the studied sequence (dots). For a zoomed view of the rectangle between stations UNI and DER, see Figure 1b.

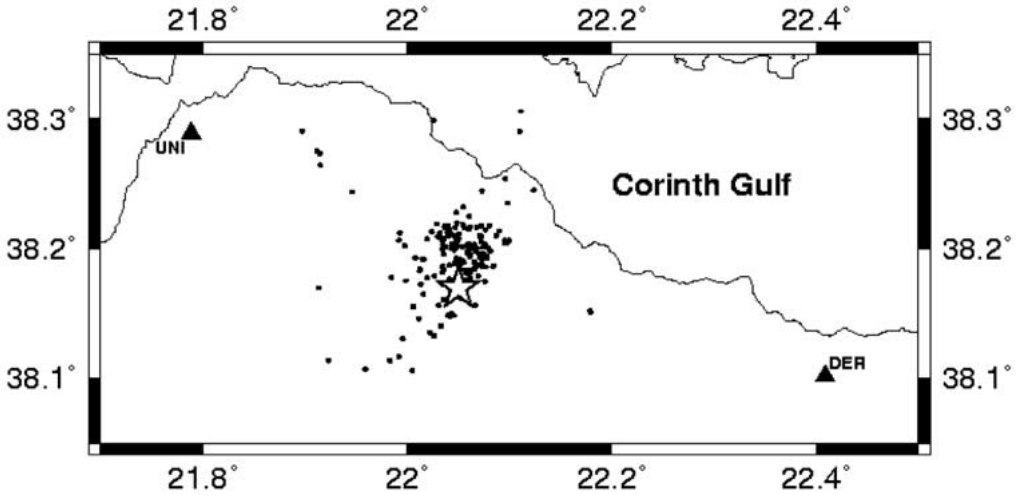

Figure 1. b. Zoom of the small rectangle area from Figure 1a. Epicenters of the whole studied sequence (dots) and the mainshock (star) are shown.

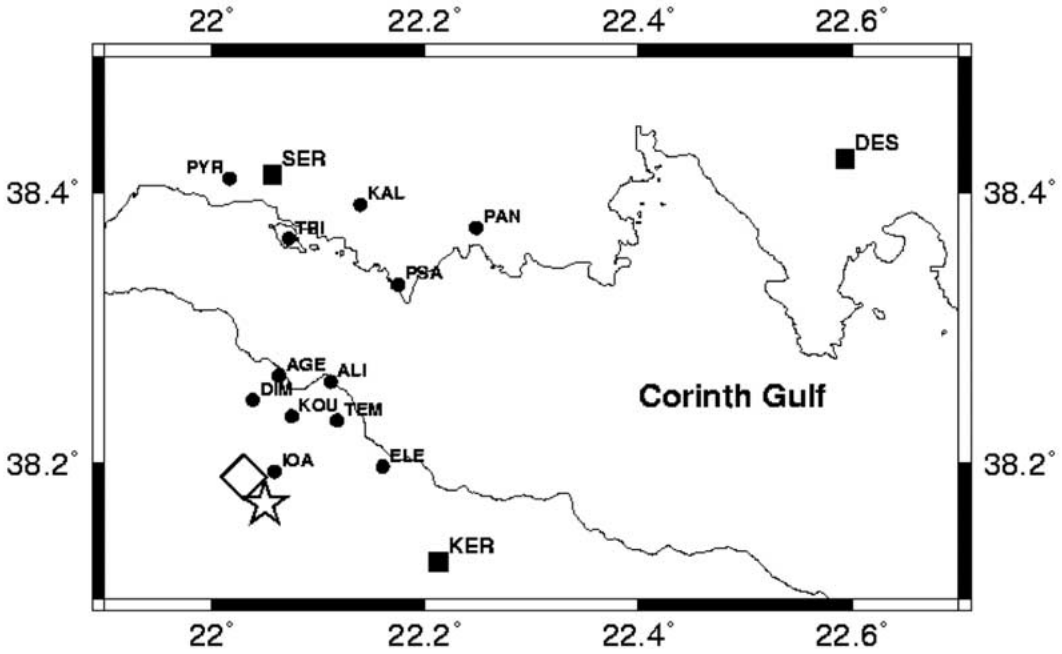

Figure 2. The western part of Corinth Gulf with 3 local stations providing waveforms for this paper (KER, SER, DES; squares), and 12 CRLNET stations (circles). The mainshock epicenter located by PATNET and CRLNET is shown by the star and diamond, respectively.

Table 2. Crustal model GMF; V_P – top and V_P – bottom denote the velocity at the layer top and bottom, respectively

Depth (km)	V_P – top (km/sec)	V_P – bottom (km/sec)
0.	2.0	5.0
2.	5.0	6.2
5.	6.2	6.4
33.	8.3	8.3

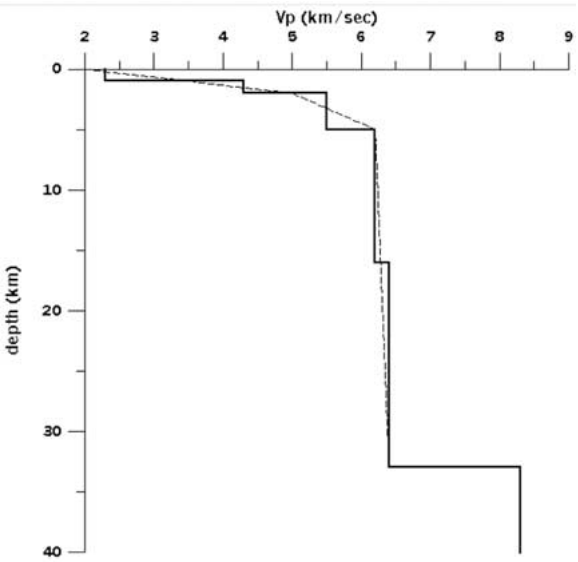

Figure 3. Crustal models GMF (dashed line) and MF (solid line) used in this paper; see also Tables 2 and 3. Model MF is used for location and waveform modeling. Model GMF, representing a close gradient approximation of MF, avoiding inter-crustal discontinuities, is used for projecting polarities on focal sphere.

cies the amplitude inversion is less sensitive to the uncertainty of the structural model.

The first-motion polarities were carefully read from the 3 above mentioned local stations (from all three components), and also from 13 short-period PATNET stations. Projecting polarities on the focal sphere is a delicate task requiring a reliable crustal model. Even models featuring low RMS location residuals may provide erroneous focal mechanisms if, with some focal depths and epicentral distances, the first arrivals are formally interpreted as head waves from inter-crustal discontinuities. This is because such discontinuities are often artifacts, and their formal presence in the 1D layered crustal models yields non-physical take-off angles (Zahradník et al., 2001). To avoid such problems we introduce a gradient model

Table 3. Crustal model MF; $V_P/V_S = 1.78$

Depth (km)	V_P (km/sec)	Q
0	2.3	300
1	4.3	300
2	5.5	300
5	6.2	300
16	6.4	300
33	8.3	1000

GMF. Model GMF is an approximation of the layered model MF (see below) used in the epicentre location and in the amplitude inversion. In model GMF the crust is represented by three layers with constant velocity gradients, followed by a velocity jump at Moho discontinuity (see Table 2 and Figure 3). The take-off angles in the gradient model were calculated with the ray-method code ANGGRA (Janský, 2001).

In ASPO method we analyze the amplitude spectra of complete 3-component displacement waveforms (duration 60 seconds), in the frequency range 0.1–0.2 Hz. The spectra are modeled by the discrete-wavenumber method of Bouchon (1981) and Coutant (1989), using crustal model MF of Table 3 and Figure 3. Model MF, whose low-velocity top layers play a key role in modeling spectra and waveforms, was obtained from Love wave dispersion curves (Novotny et al., 2001). It originated from the trial-and-error models previously used in the Patras, Corinth Gulf, and Athens regions (Plicka et al., 1998; Zahradník et al., 2001; Tselentis and Zahradník, 2000).

Three parameters are grid-searched: the strike, dip, and rake angles. As a first step, for each trial triplet of these model parameters, both the observed and synthetic (unit-moment) spectra are normalized in order to put them on a comparable amplitude level. The normalization is performed by dividing the spectra by their average value (taken over all stations, components and frequencies). As a next step, the misfit is calculated as a weighted L1 norm of the difference between the observed and synthetic amplitude spectra, summed up over all stations, components and frequencies. As introduced in Zahradník et al. (2001), the weighting is performed by dividing each member of the sum by the corresponding maximum value, i.e. $|obs_i - syn_i| / \max(obs_i, syn_i)$. Such weighting not only reduces undesired biasing effect of the largest

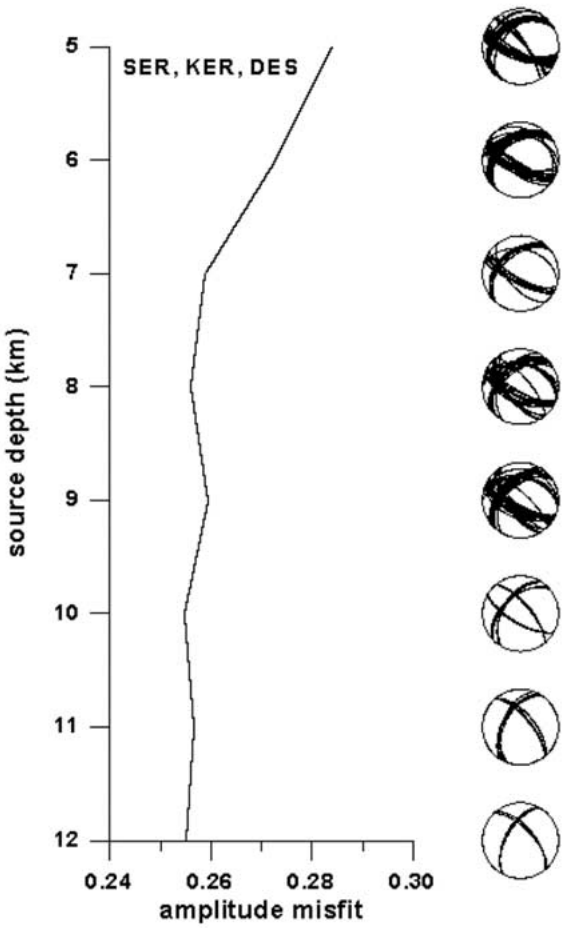

Figure 4. Variation of the amplitude-spectra misfit (minimized over strike, dip, rake) with 8 trial focal depths, and the corresponding focal mechanisms whose misfit is between minimum and minimum + 5%. Three stations are used.

amplitudes at the nearest stations, but it also adjusts the misfit values between 0 and 1. The procedure is repeated for a set of a few trial source depths (8 depths in this paper). We start with 8 depths sampling a broad depth range, then we focus to another set of 8 depths in a narrow range. Finally, the scalar moment is retrieved. It is not grid searched, since the problem is linear with respect to scalar moment. Instead of grid searching, a unit-moment synthetic spectra are calculated for the preferred mechanism and depth, and the ratio (averaged over all data) between the observed and synthetic spectra then yields the moment.

We start from jointly inverting the spectra at three stations: SER, KER, DES. Only a single very clear (compressive) first-motion polarity at SER station is required to be satisfied in this part of the study. The

Table 4. The amplitude-constrained focal mechanisms for different data sets; the preferred depth is also shown

Stations used	strike, dip, rake	strike, dip, rake
KER, SER, DES (7km)	230°, 40°, –150°	116°, 71°, –54°
SER, DES (8 km)	220°, 40°, –160°	114°, 77°, –52°
KER, SER (8 km)	270°, 20°, –140°	142°, 77°, –74°
KER, DES (9 km)	262°, 51°, +167°	360°, 80°, +40°

amplitude misfit decreases to the depth of 7 km, and then it remains nearly constant (Figure 4). As seen from the nodal lines plotted for the family of solutions whose misfit is within a fixed range, here (arbitrarily) set between minimum and minimum + 5%, the focal mechanism is stable up to 10 km. At the depth of 7 km, where the nodal lines show a small scatter, the optimum solution has strike 230°, dip = 40°, rake = –150°. However, there is also another (secondary) solution within the 5% misfit range, given by strike = 140°, dip = 60° , rake = –70°, and the conjugate solution given by strike = 284°, dip = 36°, and rake = –121°.

To decide between these two solutions, and to get insight into the uncertainty, as a next step we try to jointly invert only two stations (SER-DES, KER-SER, KER-DES), see Table 4. Physical reason for such an experiment is that we require a robust solution, not biased by some source-station path possibly deviating from the adopted 1D model. The optimum solution coming from these station subsets are consistent with each other, featuring variation of strike from 220° to 270°, of dip from 20° to 50°, and of rake from –150° to +167° (clockwise). The only other available solution, that of Swiss SED agency (Table 1), with strike 247° , dip 43° and rake –104°, fits into our uncertainty range, except for the rake. Finally, for each two-station subset, having its optimum solution we may ask if it also explains spectra at the third (omitted) station. Such an *a posteriori* check eliminates the solutions found from the KER-DES and KER-SER subsets. On the other hand, the SER-DES solution is good for the KER station, too. The SER-DES solution has a few more interesting features, see Figure 5: (i) The misfit function gives a clear preference to the source depths 6–8 km (the minimum at 8 km), (ii) The solutions are stable up to the depth of 9 km, and, moreover, they are very similar to the optimum solution found from all three stations. (iii) The secondary solution has now completely disappeared, and all solutions within the

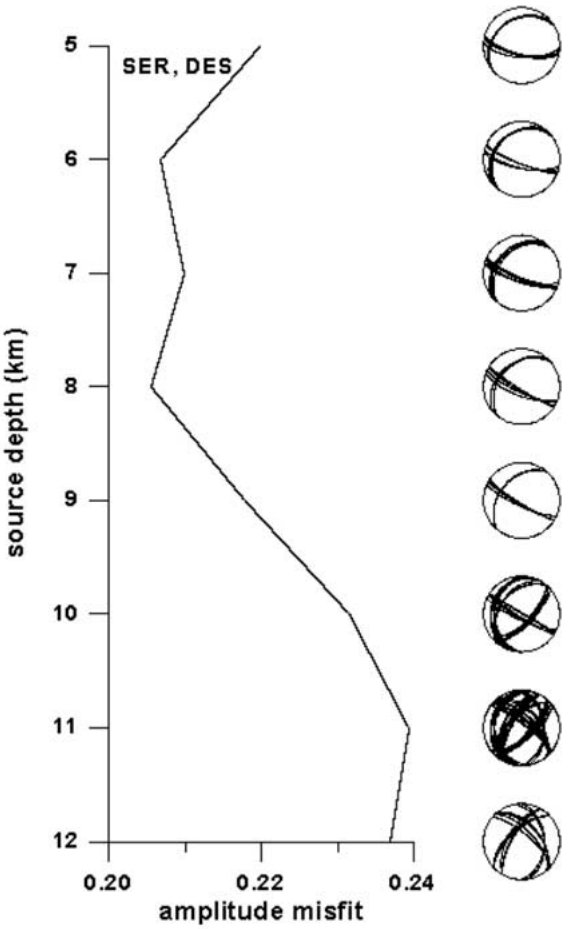

Figure 5. The same as in Figure 4, but for two stations only. Note an improved resolution, both in the focal depth and in the focal mechanism.

5% range form a single compact family (strike from 220° to 230°, dip from 35° to 40°, rake from –140° to –170°).

That is why we concentrate on the combination SER-DES, whose optimum solution at the depth of 8 km is characterized by the strike = 220°, dip = 40°, rake = –160°, and the conjugate solution 114°, 77°, –52°. The scalar moment for this solution is 2.5e15 Nm, which is equivalent to the moment magnitude M_w4.3. Let us call it final amplitude-constrained solution, or Solution 1. Because the solution is obtained from the amplitude spectra, it needs validation on waveforms (Figure 6). The KER station, not included in the SER-DES inversion, is now also employed. We find a satisfactory agreement between the observed and synthetic waveforms at all three stations and components. Station DES shows a time shift, most likely

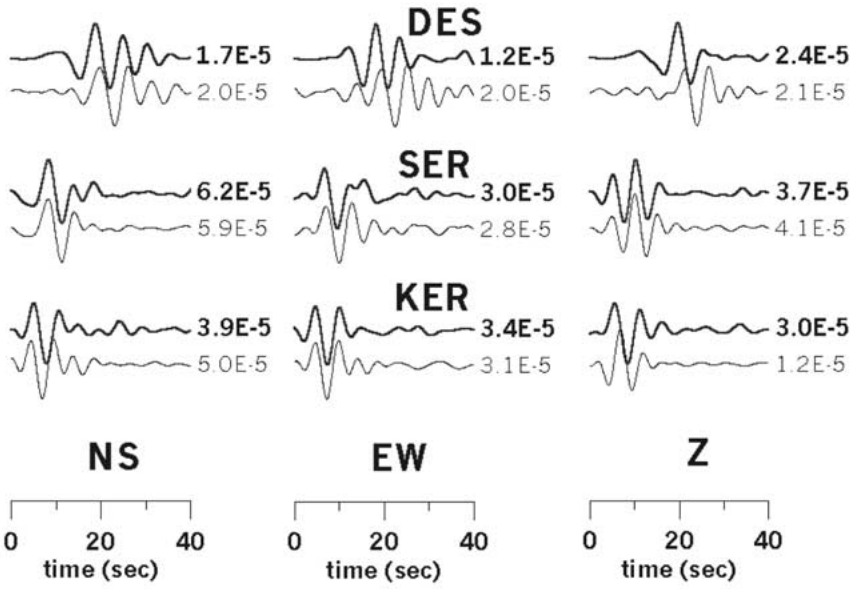

Figure 6. Comparison between the observed (top) and synthetic (bottom) displacement waveforms in the frequency range 0.1–0.2 Hz. The synthetics correspond to the focal-mechanism Solution 1. The seismograms are normalized, and their peak values (in meters) are shown on the right-hand side.

calling for a better crustal model along the corresponding source-station path, but no conclusive explanation is available.

An important part of ASPO method is the polarity constraint. However, as explained below, formal requirement to satisfy all polarities may be misleading, and finding the appropriate balance between amplitude and polarity constraint needs a great care. First, we look at all 16 first-motion polarities, and compare them with the nodal lines of the amplitude-constrained Solution 1 (the top panel in Figure 7). A strong argument supporting Solution 1 comes from DES station. Its epicentral distance is relatively small (56 km), and its negative polarity is unambiguous on all the 3 components, thanks to the digital recording of high dynamic range. At the same time, the dilatational first arrival at station DES is very weak, properly reflecting proximity of DES station to nodal line. As regards the polarity data violating Solution 1, we focus on the stations far from nodal lines and thus we find problems at the stations KEF, VOL, AGN (all at distances larger than 100 km, see Figure 1). According to the used crustal model, the first arrivals at KEF and VOL are direct P waves, while at AGN it is the Moho head wave. Therefore, we should try to explain at least the polarity disagreement at KEF and VOL. The disagreement may be related to complexity of the P-wave group. If, for example, the source process starts with a short weak pulse then, at large distances, the true first arrival may be hidden in the noise. It is not easy to recognize, during location procedure, that the true first arrival is missing at some distant stations, since its temporal separation from a later arriving stronger arrival (misinterpreted as the 'first arrival') may be as small as an acceptable location residual. An alternative (but also only speculative) explanation of the polarity disagreement at KEF and VOL may be related to the uncertainty of the crustal model. If, for example, another model would interpret these first arrivals as Moho head waves, the corresponding change in the take-off angle would make these stations compatible with Solution 1. We conclude that even if the polarities at distant stations seem 'well readable', their use is problematic at the studied magnitude level. For larger events we may find a full consistency between the amplitude-spectra and the regional first motion polarities; e.g. the M_w 5.9 Athens 1999, and the M_w6.5 Skyros 2001, earthquakes (Zahradník, 2001 and 2002).

Finally, we try to answer an interesting question, what focal mechanism would be obtained if we insist on as many polarities as possible, and, among those solutions, would prefer the minimum possible misfit between the observed and synthetic amplitude spectra. The focal mechanism like that (hereafter called Solution 2) is given by the strike = 310°, dip = 30°, rake =

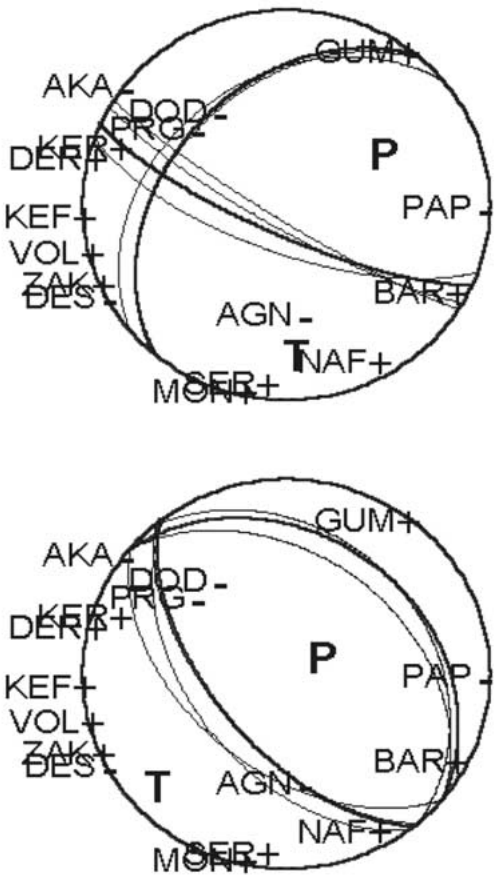

Figure 7. Nodal lines of the two focal mechanisms of this paper, compared with the first-motion polarities. Top panel – Solution 1 (from the amplitude-spectra inversion). Bottom panel – Solution 2 (constrained mainly by the polarities). Equal-area projection of the lower hemisphere. Solution 1 is strongly preferred in this paper.

–100°, and the conjugate solution 142°, 61°, –84°, see the bottom panel in Figure 7. Two stations violating Solution 2, and occurring far from nodal lines, are PAP and DES. The DES station, whose unambiguous negative polarity was already mentioned above, is important for rejecting Solution 2. However, the most clear argument against Solution 2 comes from the waveforms (Figure 8), because with this solution we get a nearly 'mirror-imaged' (= reverted) synthetics on the EW-component at the SER station, and the NS-component at the KER station. Note also that Solution 2, easily refused here, is similar to the secondary solution mentioned above in connection with the non-unique solution in Figure 4.

For all these reasons we prefer the previous Solution 1. As a next step, having the focal mechanism and depth retrieved by analyzing amplitude spectra and waveforms at the lowest available frequencies, we may try to estimate the rupture length by analyzing a broader range of frequencies. To that goal we perform forward time-domain modeling up to 5 Hz, using a triangular moment rate function of a varying duration (0.2 to 0.6 seconds, with the increment of 0.1 second). As above, crustal model MF and the discrete wavenumber method are used. Similarly to Zahradník (2002) we focus on the acceleration waveforms since the acceleration amplitude is very sensitive to the source duration. The only simple waveform is the P wave on the vertical component at SER station (KER and DES are close to nodal planes). The best fit of that waveform, band-passed between 0.1 and 5.0 Hz, was obtained for the triangle duration of 0.5 seconds; see Figure 9. Considering the possible range of the rupture propagation speed from 2 to 3 km/sec, the 0.5 second duration translates into a fault length of 1 to 1.5 km. Together with the seismic moment of 2.5e15 Nm this implies that stress drop (the static stress drop of a circular fault with the area of 1×1 or 1.5×1.5 km) was of about 2 to 6 MPa.

It is perhaps of interest to emphasize importance of this stress-drop estimate for future strong motion simulations in the studied region. Indeed, in composite source models, we synthesize large events from smaller events (subevents). When doing modeling with *synthetic* subevents, it is often not quite clear how to choose their parameters. Preference should be given to such synthetic subevents that reasonably well represent true weak events. In other words, the above results suggest that when composing a large earthquake in Corinth Gulf from $M_w \sim 4$ subevents, their stress drop should be of the order of a few MPa, but not, for example, of the order of 100 MPa. Let us mention that the peak ground motions during the 1999 Athens earthquake were also successfully explained with a composite source model whose synthetic subevents were very similar to the earthquake studied in this paper (Zahradník and Tselentis, 2002).

Before discussing possible tectonic interpretation of the studied earthquake, let us try to further check the above amplitude-constrained depth (8 km). To solve this question, additional data must be considered.

Location by a local network

We benefited from the fact that the studied earthquake occurred very close to the local network CRLNET, jointly established by the Centre Na-

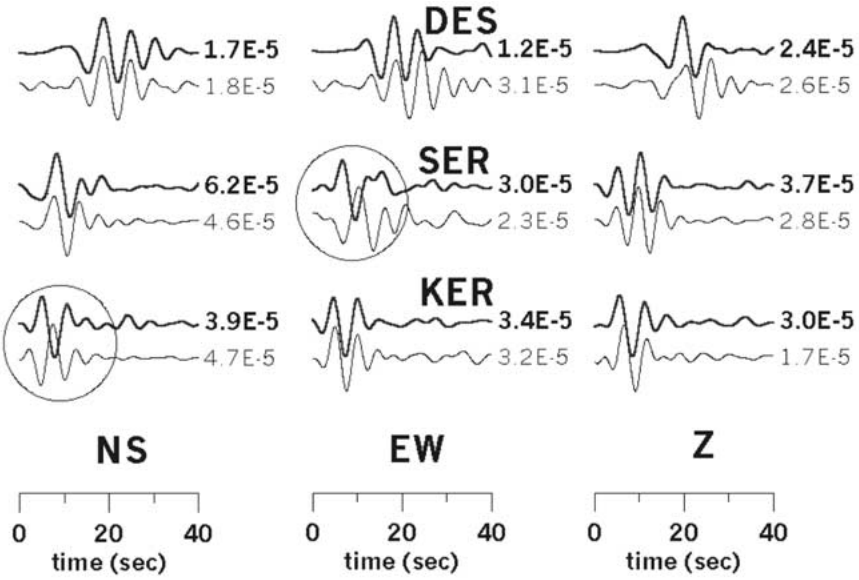

Figure 8. The same as in Figure 6, but for the focal-mechanism Solution 2. Note failures of this solution on the NS component at station KER and on the EW component at station SER.

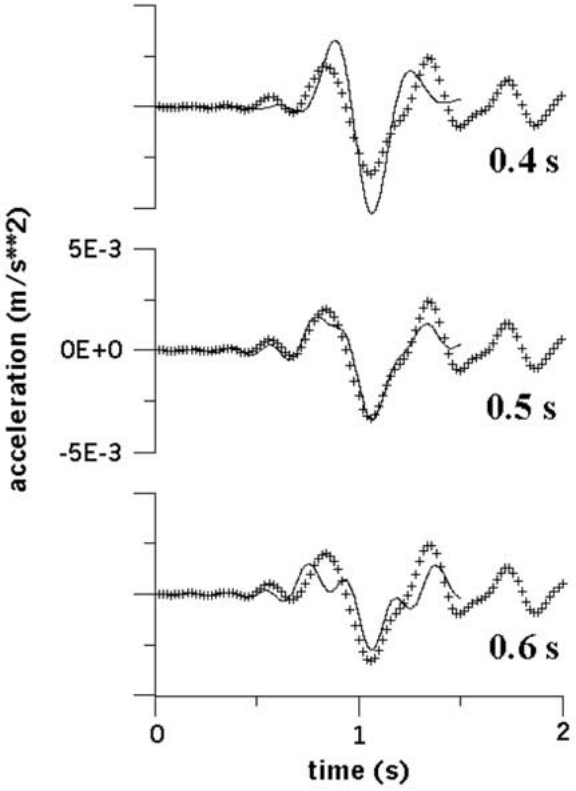

Figure 9. Comparison between the observed (crosses) and synthetic (solid line) P-wave acceleration waveforms in the frequency range 0.1–5.0 Hz for the triangular source time function of the duration 0.4 to 0.6 second. The vertical component at the SER station is shown. The best fit is found for the 0.5 second duration (middle panel).

tional de Recherche Scientifique (CNRS), France, and the University of Athens, near the city of Aegion (http://www.corinth-rift-lab.org/ and Pacchiani et al., 2002). CRLNET is composed of 12 short-period 3-component 2 Hz seismometers (Mark Products); see Figure 2. The network located all the February-July 2001 sequence, and a detailed study will be published elsewhere (Pacchiani et al., in preparation). Due to the small epicentral distances, well readable S-wave arrival times were available, to complement the P-arrivals. As a result, CRLNET provided a very compact cluster of foci, with the mainshock inside. Here we concentrate just on the April 8 mainshock (Table 1 and Figure 2). The CRLNET epicenter is very near the epicenter obtained from the PATNET data. While PATNET was unstable as regards the depth, CRLNET network provided a stable depth estimate of 5.7 km, close to the depth obtained above by inversion of the amplitude spectra (8 km). Similar shallow depths (5.4 to 7 km) were obtained also for three of the strongest aftershocks ($M_L > 3.6$), as well as for the whole sequence. We conclude that the P and S arrival times of CRLNET local network confirmed the previous waveform data of the SER, DES, KER stations, as regards the mainshock depth.

A more general implication can be formulated as follows: Although local networks are ideal for $M < 5$, they are obviously rare. An alternative solution, broadly available, is to determine the epicenter from

a regional network, while a few 3-component waveforms at local stations should be used to constrain the depth and the focal mechanism.

The CRLNET first-motion polarities (not shown here) cover a limited portion of the focal sphere only. The polarities prefer neither Solution 1 nor 2.

Tectonic discussion

The preferred fault plane solution obtained for the April 8, 2001 earthquake has a strike of 220°, dip of 40° and rake of –160° and the event occurred at ∼8km depth. The T axis for this event has an azimuth of 176° and a plunge of 67°. This is consistent with the ∼N10° regional extension obtained from GPS and fault plane solutions of larger events. Major faults outcropping on the southern coast of the western Corinth Gulf are normal faults with ESE-WNW orientation and a steep (∼60°) dip to the NNE. None of the two nodal planes obtained for the April 8 event agrees with these outcropping structures. It is also impossible to relate this event to a possible detachment zone at a depth about 10 km. The high resolution relocation of the *whole sequence* (Pacchianni et al., 2002 and a paper in preparation) will probably help to better interpret this event in the tectonic framework. In particular, we believe that the detailed spatial distribution of the sequence will provide a focused image of several underground tectonic structures, some of them possibly related to the mainshock focal mechanism.

Conclusion

In February-July 2001, an earthquake sequence comprising almost 2000 events occurred at about 10 km south of Aegion, the town heavily damaged by the M_L 6.2 earthquake of 1995. This paper deals with 171 events of M_L from 1.8 to 4.7, recorded and located by the regional short-period network of the University of Patras, PATNET, and it concentrates on the April 8, 2001, mainshock M_L4.7.

Several methods were used to relocate the sequence, mainly based on the P-wave readings. The epicenter distribution from all the methods was nearly the same, but the depth determination was strongly unstable (e.g., the mainshock depth ranged from 0 to 20 km).

To retrieve the focal mechanism of the mainshock, the amplitude spectra of complete waveforms were inverted in the range 0.1 to 0.2 Hz, below the corner frequency, using a grid search of the strike, dip and rake, at several trial depths. Three local stations, KER, SER, DES (at the epicentral distances of 17, 26 and 56 km) were employed. The preferred solution, validated by forward waveform modeling, is given by the strike = 220°, dip = 40°, rake = -160^o(conjugate solution 114°, 77°, –52°), and the depth = 8 km. The scalar seismic moment is 2.5e15 Nm.

As indicated by forward time-domain modeling up to 5 Hz, the source moment rate can be simulated by a triangle of the 0.5 second duration. The 0.5 second duration is equivalent to 1–1.5 km fault length, or static stress drop of 2–6 MPa. It is important for future strong motion predictions in the Aegion region. Indeed, if the composite source models require synthetic M∼4 subevents, their stress drop can be chosen consistently with the present result. However, more validation is needed, because the above mentioned stress drop assessment was made from P wave at vertical component of the SER station record only.

To further check the mainshock depth, a 12-station local network CRLNET was additionally involved. Thanks to 3-component recording, and short epicentral distances, both P- and S-wave arrivals were available. The epicenter of the mainshock was found very near to that of PATNET results (Table 1, Figure 2), and the depth of about 6 km confirmed the previous amplitude-constrained estimate obtained from the three local stations.

The failure of the PATNET depth estimate for the mainshock was most likely caused by complete unavailability of the S-wave readings. The distant PATNET stations (> 100 km) provided also problematic first-motion polarities. It seems that a generally valid recommendation for weak events can be formulated as follows: If a local network is not available, locate the epicenter in a regional short-period network, and add a few local 3-component waveforms for constraining the depth and focal mechanism.

Although the studied earthquake is consistent with the known pattern of the regional deformation (i.e. the approximately ∼N10° extension), neither of the two nodal planes agrees with major outcropping structures of the southern coast of the western Corinth Gulf. The relation of the event to deeper blind faults remains open. It is impossible to relate this event to the detachment zone, possibly existing at a depth of about 10 km. It is possible that the event occurred on older structures reactivated in the present stress field. This hypothesis will be further addressed by the high-resolution CRL-

NET relocation of the entire sequence (Pacchiani et al., in preparation).

Acknowledgements

The first-named author thanks to Prof. G. Akis Tselentis for his long-lasting co-operation and joint operation of seismic stations SER and KER. The work was supported by the following grants: NATO Collaborative Linkage grant EST.CLG.976035; EU PRESAP project EVG1-CT-1999-00001, and the Czech Republic research projects – MSM 113200004, GACR 205/00/0902 (submitted version), and GACR 205/03/1047 (revised version). Installation of the CRLNET network was funded by INSU-CNRS (France), while its maintenance and data analysis was possible through the EVC CORSEIS project EVG1-1999-00002.

References

Armijo, R., Meyer, B., King, G., Rigo, A. and Papanastassiou, D., 1996, Quaternary evolution of the Corinth rift and its implications for the late Cenozoic evolution of the Aegean, *Geophys. J. Int.* **126**, 11–53.

Bernard, P., Briole, P., Meyer, B., Lyon-Caen, H., Gomez, J.-M., Tiberi, C., Berge, C., Cattin, R., Hatzfeld, D., Lachet., C., Lebrun, B., Deschamps, A., Courboulex, F., Laroque, C., Rigo, A., Massonnet, D., Papadimitriou, P., Kassaras, J., Diagourtas, D., Makropoulos, K., Veis, G., Papazisi, E., Mitsakaki, C., Karakostas, V., Papadimitriou, E., Papanastassiou, D., Chouliaras, G. and Stavrakakis, G., 1997, The Ms=6.2, June 15, 1995 Aigion Earthquake (Greece): Evidence for Low Angle Normal Faulting in the Corinth Rift, *J. Seismol.* **1**, 131–150.

Bouchon, M., 1981, A simple method to calculate Green's functions for elastic layered media, *Bull. Seism. Soc. Am.* **71**, 959–971.

Briole, P., Rigo, A., Lyon-Caen, H., Ruegg, J.C., Papazissi, K., Mitsakaki, C., Balodimou, A., Veis, G., Hatzfeld, D. and Deschamps, A., 2000, Active deformation of the Corinth rift, Greece: results from repeated Global Positioning System surveys between 1990 and 1995, *J. Geophys. Res.* **105**, 25605–25625.

Clarke, P.J., Davies, R.R., England, P.C., Parsons, B.E., Billiris, H., Paradissis, D., Veis, G., Denys, P.H., Cross, P.A., Ashkenazi, V., Bingley, R., 1997, Geodetic estimation of seismic hazard in the Gulf of Corinth, *Geophys. Res. Lett.* **24**, 1303–1306.

Coutant, O., 1989, Program of Numerical Simulation AXITRA. Research report, LGIT, Grenoble.

Hatzfeld, D., Karakostas, V., Ziazia, M., Kassaras, I., Papadimitriou, E., Makropoulos, K., Voulgaris, N. and Papaioannou, C., 2000, Microseismicity and faulting geometry in the Gulf of Corinth (Greece), *Geophys. J. Int.* **141**, 438–456.

Janský, J., 2000, Grid search hypocentral location method in simple 1-D media, *Acta Montana* IRSM AS CR, Series A **118**, 71–84.

Janský, J., 2001, Ray-method calculations of the travel times and take-off angles in gradient models, program ANGGRA, Research report, Dept. of Geophysics, Faculty of Math. and Phys., Charles University, Prague.

Janský, J., Zahradník, J., Sokos, E., Serpetsidaki, A. and Tselentis, A., Relocation of the 2001 earthquake sequence in Aegion, Greece, using grid search, *Studia geoph. et geod.*, submitted.

Lee, W.H.K. and Valdes, C.M., 1989, Hypo71PC Toolbox for seismic data acquisition, processing, and analysis, IASPEI & SSA.

Lyon-Caen, H. and Rigo, A., 1997, Seismological observations in the Gulf of Corinth, Proceedings of the 1st workshop on the development of a multiborehole observatory at the Gulf of Corinth, ICDP (International Continental Drilling Project) report, http://www.corinth-rift-lab.org/index_en.html

Novotný, O., Zahradník, J. and Tselentis, G.-A., 2001, North-Western Turkey earthquakes and the crustal structure inferred from surface waves observed in Western Greece, *Bull. Seism. Soc. Am.* **91**, 875–879.

Pacchiani, F., Lyon-Caen, H., Bourouis, S., Bernard P. and Deschamps, A., 2002, Cluster relocation in the Corinth rift and fault geometry, book of abstracts, XXVIII Gen. Ass. ESC, Genoa, 1–6 September 2002.

Plicka, V., Sokos, E., Tselentis, G.-A. and Zahradník, J., 1998, The Patras earthquake (July 14, 1993) – relative roles of source, path and site effects, *J. Seismol.* **2,** 337–349.

Rietbrock, A., Tiberi, C., Scherbaum, F. and Lyon-Caen, H., 1996, Seismic slip on a low angle normal fault in the Gulf of Corinth: evidence from high resolution cluster analysis of microearthquakes, *Geophys. Res. Lett.* **14**, 1817–1820.

Rigo, A., Lyon-Caen, H., Armijo, R., Deschamps, A., Hatzfeld, D., Makropoulos, K., Papadimitriou, P. and Kassaras, I., 1996, A microseismic study in the western part of the Gulf of Corinth (Greece): implications for large scale normal faulting mechanisms, *Geophys. J. Int.* **126**, 663–688.

Tselentis, G.-A., Melis, N., Sokos, E. and Papatsimpa, K., 1996, The Egion June 15, 1995 (6.2 ML) earthquake, Western Greece, *Pure appl. geophys.* **147**, 83–98.

Tselentis, G.-A. and Zahradník, J., 2000, The Athens earthquake of September 7, 1999, *Bull. Seism. Soc. Am.* **90**, 1143–1160.

Zahradník, J., Janskí, J. and Papatsimpa, K., 2001, Focal mechanisms of weak earthquakes from amplitude spectra and polarities, *Pure appl. geophys.* **158**, 647–665.

Zahradník, J., 2001, Focal mechanism of the Athens 1999 earthquake by ASPO method, Research report, Dept. of Geophysics, Faculty of Math. and Phys., Charles University, Prague; see also http://sei30.karlov.mff.cuni.cz.

Zahradník, J., 2002, Modeling the Skyros island, Aegean Sea Mw=6.5 earthquake of July 26, 2001, *Studia geoph. et geod.***46**, 753–771.

Zahradník, J. and Tselentis G.-A., 2002., Modeling strong-motion accelerograms by PEXT method, application to the Athens 1999 earthquake, Proc. XXVIII Gen. Ass. ESC, Genoa, 1–6 September 2002 (CD-ROM). See http://seis30.karlov.mff.cuni.cz.